ANZIAM J. **67, e32** (2025), 1–22
doi:10.1017/S144618112510014X

WAVE INTERACTION WITH AN H-SHAPED SUBMERGED BREAKWATER

R. B. KALIGATLA[1], P. PANJA[1] and B. N. MANDAL[2]

(Received 27 October, 2024; accepted 26 April, 2025)

Abstract

We present a study of oblique-wave scattering by an H-shaped breakwater submerged in deep water. The H-shaped breakwater is designed using two thin vertical plates connected by a thin horizontal plate. The velocity potentials that describe the wave motion in different regions are expressed using the Havelock expansion. Two first-kind Fredholm-type integral equations are derived by applying the continuity of fluid velocity and pressure at the interface for the horizontal component of fluid velocity across the gap below and above the breakwater. The coefficients of wave reflection and transmission are derived in explicit forms that require the solution of integral equations. The solutions of integral equations are obtained by employing the Galerkin approximation that involves simple polynomials. In some limiting cases, wave scattering by submerged $\sqcap$ and $\sqcup$-shaped breakwaters is also studied. The correctness of the results is verified by comparing them with existing results reproduced in a limiting case and checking the wave energy balance equation. The results reveal that the H-, $\sqcap$- and $\sqcup$-shaped breakwaters show low wave transmission for most incident wavelengths. The horizontal plate between the vertical plates accounts for this low wave transmission. Wave forces and the overturning moment are also calculated. These breakwaters may be used in water regions that require low wave transmission.

2020 *Mathematics subject classification*: 76B15.

Keywords and phrases: H-shaped breakwater, integral equations, wave scattering, Galerkin approximation, wave force, overturning moment.

1. Introduction

In recent times, the study of wave scattering by breakwaters with improved design has received increasing interest from investigators because new configurations have been found to outperform conventional breakwaters that have simple configurations.

[1]Department of Mathematics and Computing, Indian Institute of Technology (ISM) Dhanbad, Dhanbad 826004, India; e-mail: ramana@iitism.ac.in, panjapapita1997@gmail.com
[2]Physics and Applied Mathematics Unit, Indian Statistical Institute, 203, B.T. Road, Kolkata 700108, India; e-mail: bnm2006@rediffmail.com
© The Author(s), 2025. Published by Cambridge University Press on behalf of the Australian Mathematical Publishing Association Inc.

https://doi.org/10.1017/S144618112510014X Published online by Cambridge University Press

The improved designs of breakwaters involve multiple solid or thin-plate structures or their combinations with permeable and/or impermeable features. The addition of thin plates to rectangular structures is a current study of the wave protection performance of breakwaters. Vertical thin plates increase wave reflection and dissipate turbulent energy [32], and horizontal thin plates (or bilge keels) reduce the rolling motion of breakwater and the amplitude of radiated waves [2]. For example, ⊓ and T-shaped breakwaters fall under this category. Furthermore, the H-shaped breakwater is a typical one and was investigated experimentally as a free-surface breakwater by Neelamani and Vedagiri [25] for regular and irregular wave scattering. In their study, the H-shaped breakwater was found to reduce the wave transmission coefficient by up to 0.2 in the regular wave regime and at different locations of the submerged barrier closer to deep-water conditions. In addition, this type of breakwater was not allowed in shallow-water conditions. Nishad et al. [26] developed a dual boundary element method (BEM) for a porous H-shaped breakwater to study wave scattering. Their findings indicate that the H-shaped breakwater increases wave transmission, and reduces wave reflection and forces. It was also found that the breakwater reduces wave transmission by twenty percent without an increase in horizontal force in shallow water. Panda et al. [27] used multi-domain BEM to investigate wave trapping and dissipation performance of the H-shaped breakwater combined with two vertical/inclined barriers. The width of the flange in the breakwater was found to control wave transmission, and thus optimal wave trapping and maximum wave energy dissipation were achieved. Neelamani and Rajendran [24] studied wave scattering by a submerged T-type breakwater and found that it reduces wave transmission effectively in regions close to deep-water conditions. Günaydın and Kabdaşlı [9] tested experimentally the scattering performance of the U-shaped breakwater (⊔) in different submerged regimes for regular and irregular waves. The study of Gesraha [8] for the ⊓-shaped breakwater and that of Deng et al. [5] for the T-shaped breakwater show directives for lower wave transmission and reductions in wave-induced motions. In general, a rectangular box-type breakwater with inclined attached plate plays a crucial role in reducing wave transmission [17]. The angle of inclination of the attached plates may suitably be chosen for engineering applications. Furthermore, the study of Kaligatla et al. [12] and Singh et al. [33] on wave scattering by ⊓-shaped breakwaters in deep and finite depth water again confirmed the findings of Gesraha [8] for wave scattering employing a different method. Teh [34] made a comprehensive comparison with respect to the scattering performance between many different types of breakwater. In addition, some new cross-sectional shapes of the breakwater and their utility are illustrated by Wang and Nguyen [37]. The study of Mohapatra et al. [21] concerning wave scattering and radiation by a simple conventional three-dimensional (3D) rectangular box offers future directions for considering improved designs with a 3D rectangular box as in the preceding literature.

The conversion of mixed boundary value problems that arise in water wave problems, assuming linear theory, to integral equations has been a long practice since the time of Ursell [36]. Ursell derived elegantly first-kind Cauchy-type singular

https://doi.org/10.1017/S144618112510014X Published online by Cambridge University Press

integral equations to obtain wave reflection and transmission coefficients of surface piercing and fully submerged vertical thin barriers in deep water. Subsequently, wave scattering by vertical barriers of several configurations has been treated by integral equation methods in finite and infinite depth of water (for example, see [1, 6, 29, 30]). Wave scattering by inclined barriers was treated by hypersingular integral equations (see [20, 28] and others).

The integral equation method has been widely used not only for several single-barrier scattering problems, but also for multiple-barrier scattering problems. The methods developed by investigators are indeed assisting us in deriving integral equations for newly designed breakwaters and serving as benchmark results to check the correctness of the developed methods. Here, we discuss some useful integral equation methods applied to multiple barriers. The scattering of water waves by two vertical barriers that pierce the free surface of deep water was treated by Levine and Rodemich [14] employing the Schwarz–Christoffel transformation from complex-variable theory. They derived the reflection and transmission coefficients with cumbersome analysis. In a similar fashion, Jarvis [11] derived an explicit expression of the reflection and transmission coefficients arising from two fully submerged parallel barriers extending infinitely downward from a fixed point below the free surface. Evans and Morris [7] derived complementary approximations of the scattering coefficients of two-surface piercing barriers in infinite depth water and showed that complete reflection could be possible at certain incident wavelengths. De et al. [3] and [4] alternatively proposed an Abel integral equation approach to obtain simple explicit forms of the reflection and transmission coefficients of two surface-piercing barriers and two fully submerged barriers. Their integral equation formulation is much simpler than that of Levine and Rodemich [14], and Jarvis [11], and the explicit forms of the derived scattering coefficients are easy to compute. Two vertical parallel barriers with equal lengths were reported to produce zero reflection or total transmission for certain incident wavelengths. However, this is not the case with vertical barriers of unequal lengths, that is, nonzero reflection occurs for these type barriers (see [18] for the matched eigenfunction expansion and [31] for the first-kind Fredholm-type integral equations in the mathematical analysis).

Many human activities have been shifted to offshore regions due to high wave agitations by sloshing effects in shallow-water regions. As a result, the number of offshore structures increases and the diversity of designs is rapidly growing. Nowadays, many breakwater structures have been located in deep-water locations to protect offshore operations. A breakwater in deep water is meant to be considered deep-water breakwater, but not for the breakwater in shallow-water regions at greater depths. The necessity of designing deep-water breakwaters in the present environmental conditions is emphasized and illustrated by Nederstigt [23] for several reasons. In this article, we study wave scattering by an H-shaped breakwater submerged in deep water, taking into account the advantages of horizontal and vertical plates discussed above. The H-shaped breakwater is designed by two identical thin plates in vertical position connected by a thin horizontal plate. The velocity potential formulation

https://doi.org/10.1017/S144618112510014X Published online by Cambridge University Press

for fluid motion and the linear theory for wave motion are adopted. The method of integral equation constructed in this article closely follows the method in [12]. The H-shaped breakwater is impermeable and has geometrical symmetry. The symmetry enables us to limit the mathematical analysis to a half-domain and to a half-plane. The velocity potential is expressed by the Havelock expansion in each region within and outside the breakwater. Using the continuity of fluid velocity and pressure at the interface, integral equations are derived for the horizontal component of fluid velocity across the gaps above and below the breakwater. Explicit expressions of the wave reflection and transmission coefficients are derived. These involve the solution of integral equations. The solutions are obtained by employing the method of the Galerkin approximation [12]. Furthermore, submerged ⊔- and ⊓-shaped breakwaters are considered limiting cases. The wave reflection and transmission coefficients of all these breakwaters are analysed for different wave and breakwater parameters to determine their scattering performance. Also, the proposed method is validated with the pre-established benchmark results. The results derived from this study may be useful for the design of breakwaters in water regions where low wave transmission is required.

2. Mathematical formulation

Figure 1 shows the schematic of the H-shaped breakwater submerged in deep water. The impermeable H-shaped breakwater comprises two vertical thin plates connected by a horizontal thin plate. To avoid edge effects, the breakwater is assumed to be indefinitely long in the z-direction. In other dimensions, the breakwater has width $2b$, depth of submersion c and the breakwater occupies up to d. Thus, the wave-scattering problem in this article is formulated as a two-dimensional problem rather than a three-dimensional problem. Since the H-shaped breakwater has a symmetrical configuration, the entire fluid region is split into three regions, as shown in Figure 1. Waves on the water surface shall impinge on the breakwater either from the positive x-direction or negative x-direction, and the wave scattering is identical by the symmetrical breakwater. The fluid motion is governed by the Laplace equation, which results from the equation of continuity under the assumptions of an incompressible and inviscid fluid with irrotational motion. Furthermore, waves are assumed to have small wave steepness. When a train of monochromatic waves, incoming from the positive x-direction, impinge on the fixed H-shaped breakwater obliquely at an angle α, they will be scattered in different directions. So, the problem involves determining the wave reflection and transmission amplitudes. Because the geometry of the breakwater is invariant in the z-direction, we seek a periodic solution in the z-direction. The z part can be separated from the solution in this case.

Based on the fluid and wave assumptions, we write the velocity potential in the form $\Phi(x, y, z, t) = \mathrm{Re}[\phi(x, y)e^{i(\upsilon z-\omega t)}]$, where $i = \sqrt{-1}$. Here, $\upsilon = K \sin\alpha$ with wavenumber K, and ω is the angular frequency and t is time. In deep water, the wavenumber $K = \omega^2/g$ with gravitational constant g. The expression $e^{i(\upsilon z-\omega t)}$ is suppressed

https://doi.org/10.1017/S144618112510014X Published online by Cambridge University Press

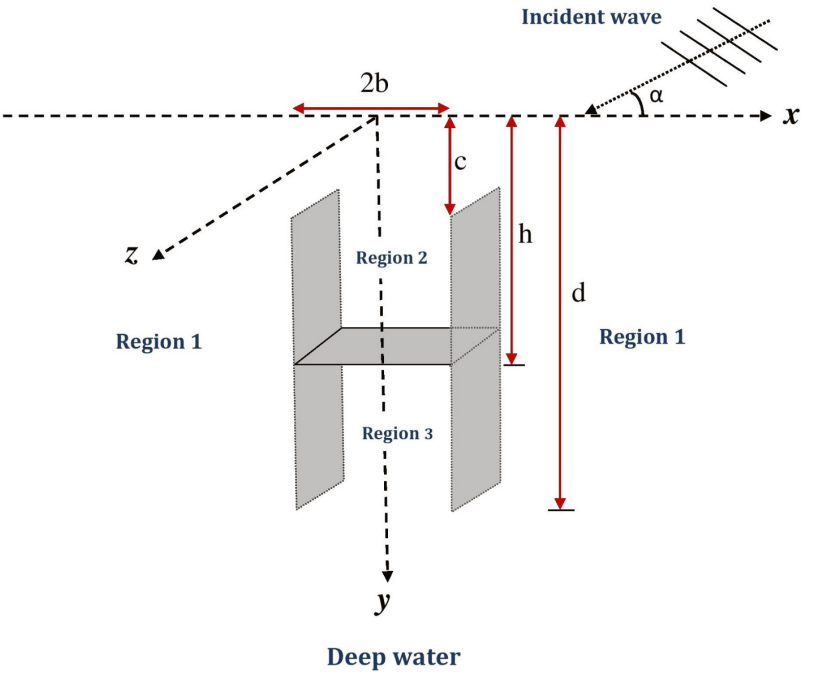


FIGURE 1. Sketch of an H-shaped breakwater submerged in deep water. Region 1: $\{(x,y) : b < x < \infty, 0 < y < \infty\}$ and $\{(x,y) : -\infty < x < -b, 0 < y < \infty\}$; Region 2: $\{(x,y) : 0 < x < b, 0 < y < h\}$ and $\{(x,y) : -b < x < 0, 0 < y < h\}$; Region 3: $\{(x,y) : 0 < x < b, h < y < \infty\}$ and $\{(x,y) : -b < x < 0, h < y < \infty\}$. In each region, $-\infty < z < \infty$ is assumed.

throughout the analysis. Since the breakwater has an invariant configuration in the z-direction, matching of the solutions at the interface between regions is possible by Snell's law [13].

The entire fluid motion is governed by the modified Helmholtz equation

$$(\partial_x^2 + \partial_y^2 - \upsilon^2)\phi = 0, \quad -\infty < x < \infty, \ 0 < y < \infty, \tag{2.1}$$

where ∂_x^2 and ∂_y^2 are the second-order partial derivatives with respect to variables x and y, respectively. The free-surface boundary condition is

$$(\partial_y + K)\phi = 0 \quad \text{on } y = 0. \tag{2.2}$$

Conditions on each vertical side of the breakwater are

$$\partial_x\phi = 0 \quad \text{on } \ x = \pm b, \ y \in (c,d) \text{ in Region 1}, \tag{2.3}$$

$$\partial_x\phi = 0 \quad \text{on } \ x = \pm b, \ y \in (c,h) \text{ in Region 2}, \tag{2.4}$$

$$\partial_x\phi = 0 \quad \text{on } \ x = \pm b, \ y \in (h,d) \text{ in Region 3}. \tag{2.5}$$

https://doi.org/10.1017/S144618112510014X Published online by Cambridge University Press

Conditions on the horizontal side of the breakwater are

$$\partial_y \phi = 0 \quad \text{on} \quad y = h, \ x \in (-b, b) \text{ in Region 2}, \tag{2.6}$$

$$\partial_y \phi = 0 \quad \text{on} \quad y = h, \ x \in (-b, b) \text{ in Region 3}. \tag{2.7}$$

The deep-water condition is

$$\phi, \partial_x \phi, \partial_y \phi \to 0 \quad \text{as } y \to \infty \text{ for } |x| < \infty. \tag{2.8}$$

The edge conditions [16] are

$$\begin{aligned} r^{1/2}(\partial_x \phi, \partial_y \phi) \quad &\text{is bounded as } r \to 0, \\ s^{1/2}(\partial_x \phi, \partial_y \phi) \quad &\text{is bounded as } s \to 0, \end{aligned} \tag{2.9}$$

where $r = \sqrt{(x \mp b)^2 + (y - c)^2}$ and $s = \sqrt{(x \pm b)^2 + (y - d)^2}$.

The far-field conditions are

$$\phi = \begin{cases} \phi^{inc}(x, y) + R\phi^{inc}(-x, y) & \text{as } x \to \infty, \\ T\phi^{inc}(x, y) & \text{as } x \to -\infty, \end{cases} \tag{2.10}$$

where the incident wave $\phi^{inc}(x, y) = 2e^{-Ky - i\mu(x-b)}$ with $\mu = K \cos \alpha$. The constants R and T are the coefficients of wave reflection and transmission to be determined.

3. Reduction to integral equations

When the breakwater geometry is symmetric with respect to some coordinate axis, the velocity potential $\phi(x, y)$ is usually split into symmetric and antisymmetric functions (see [15, Ch. 2]). Here, we write the function $\phi(x, y)$ as the sum of symmetric and antisymmetric parts $\psi^s(x, y)$ and $\psi^a(x, y)$, respectively. That is,

$$\phi(x, y) = \psi^s(x, y) + \psi^a(x, y),$$

where

$$\psi^s(-x, y) = \psi^s(x, y) \quad \text{and} \quad \psi^a(-x, y) = -\psi^a(x, y). \tag{3.1}$$

Thus, the domain of the scattering problem is restricted to the region $x \geq 0$ only. Now, $\psi^s(x, y)$ and $\psi^a(x, y)$ satisfy (2.1)–(2.7). From (3.1),

$$\partial_x \psi^s(0, y) = 0, \quad 0 < y < \infty, \tag{3.2}$$

$$\psi^a(0, y) = 0, \quad 0 < y < \infty. \tag{3.3}$$

Let the behaviour of $\psi^{s,a}(x, y)$ be represented by

$$\psi^{s,a}(x, y) \approx e^{-Ky}\{e^{-i\mu(x-b)} + R^{s,a} e^{i\mu(x-b)}\} \quad \text{as } x \to \infty, \tag{3.4}$$

where $\psi^{s,a}(x, y)$ is read as $(\psi^s(x, y), \psi^a(x, y))$. The constants R^s and R^a are to be determined. From (2.10) and (3.4), we find that

$$(R, T) = \tfrac{1}{2}(R^s \pm R^a)e^{-2i\mu b}.$$

https://doi.org/10.1017/S144618112510014X Published online by Cambridge University Press

Now, the Havelock expansions [10] of $\psi^{s,a}(x,y)$ satisfying (2.1)–(2.8), (3.2) and (3.3) (for $x \geq 0$) are the following. The expansions are usually deduced by means of separation of variables in each region.

Region 1 ($x > b,\ 0 < y < \infty$):

$$\psi^{s,a}(x,y) = e^{-Ky}\{e^{-i\mu(x-b)} + R^{s,a}e^{i\mu(x-b)}\} + \int_0^\infty A^{s,a}(\xi)S(\xi,y)e^{-\xi_1(x-b)}\,d\xi, \tag{3.5}$$

where $S(\xi,y) = \xi\cos(\xi y) - K\sin(\xi y)$ and $\xi_1 = \sqrt{\upsilon^2 + \xi^2}$.

Region 2 ($0 < x < b,\ 0 < y < h$):

$$\begin{pmatrix}\psi^s(x,y)\\ \psi^a(x,y)\end{pmatrix} = \begin{pmatrix}C_0^s\cos r_0 x\\ C_0^a\sin r_0 x\end{pmatrix}\frac{\cosh\alpha_0(h-y)}{\cosh\alpha_0 h} + \sum_{n=1}^\infty \begin{pmatrix}C_n^s\cosh(r_n x)\\ C_n^a\sinh(r_n x)\end{pmatrix}\cos\alpha_n(h-y), \tag{3.6}$$

where $\alpha_0, \pm i\alpha_n\ (n = 1,2,3,\ldots)$ satisfy $\alpha\tanh\alpha h - K = 0$, $r_0 = \sqrt{\alpha_0^2 - \upsilon^2}$, $r_n = \sqrt{\alpha_n^2 + \upsilon^2}$, $n = 1,2,3,\ldots$.

Region 3 ($0 < x < b,\ h < y < \infty$):

$$\begin{pmatrix}\psi^s(x,y)\\ \psi^a(x,y)\end{pmatrix} = \begin{pmatrix}\displaystyle\int_0^\infty B^s(\xi)\cosh(\xi_1 x)\cos\xi(y-h)\,d\xi\\ \displaystyle\int_0^\infty B^a(\xi)\sinh(\xi_1 x)\cos\xi(y-h)\,d\xi\end{pmatrix}. \tag{3.7}$$

Let $\zeta^{s,a}(y)$ be the horizontal component of fluid velocity across the line $x = b$, that is,

$$\zeta^{s,a}(y) = \partial_x\psi^{s,a}(b+0,y) \quad \text{for } y \in (0,\infty), \tag{3.8}$$

then

$$\zeta^{s,a}(y) = 0 \quad \text{for } y \in (c,d).$$

Also, since

$$\zeta^{s,a}(y) = \partial_x\psi^{s,a}(b-0,y) \quad \text{for } y \in (0,h)\cup(h,\infty), \tag{3.9}$$

we find that

$$\zeta^{s,a}(y) = 0 \quad \text{for } y \in (c,h)\cup(h,d).$$

From the edge condition (2.9), we find that

$$\zeta^{s,a}(y) = \begin{cases} O(|y-c|^{-1/2}) & \text{as } y \to c,\\ O(|y-d|^{-1/2}) & \text{as } y \to d.\end{cases}$$

https://doi.org/10.1017/S144618112510014X Published online by Cambridge University Press

On using the expansion (3.5) for $\psi^{s,a}(y)$ in (3.8) and by Havelock's inversion formula,

$$\begin{aligned} 1 - R^{s,a} &= \frac{2iK}{\mu}\left\{\int_0^c \zeta^{s,a}(u)e^{-Ku}\,du + \int_d^\infty \zeta^{s,a}(u)e^{-Ku}\,du\right\},\\ A^{s,a}(\xi) &= -\frac{2}{\pi\xi_1(\xi^2+K^2)}\left\{\int_0^c \zeta^{s,a}(u)S(\xi,u)\,du + \int_d^\infty \zeta^{s,a}(u)S(\xi,u)\,du\right\}. \end{aligned} \tag{3.10}$$

In the same way, on using the expansion (3.6) for $\psi^{s,a}(y)$ in (3.9) and by Havelock's inversion formula, we obtain the integral relations

$$\begin{aligned} C_0^s &= -\frac{4\alpha_0\cosh\alpha_0 h}{r_0(2\alpha_0 h+\sinh 2\alpha_0 h)\sin r_0 b}\int_0^c \zeta^s(u)\cosh\alpha_0(h-u)\,du,\\ C_0^a &= \frac{4\alpha_0\cosh\alpha_0 h}{r_0(2\alpha_0 h+\sinh 2\alpha_0 h)\cos r_0 b}\int_0^c \zeta^a(u)\cosh\alpha_0(h-u)\,du,\\ C_n^s &= \frac{4\alpha_n}{r_n(2\alpha_n h+\sin 2\alpha_n h)\sinh r_n b}\int_0^c \zeta^s(u)\cos\alpha_n(h-u)\,du, \quad n=1,2,3,\ldots,\\ C_n^a &= \frac{4\alpha_n}{r_n(2\alpha_n h+\sin 2\alpha_n h)\cosh r_n b}\int_0^c \zeta^a(u)\cos\alpha_n(h-u)\,du, \quad n=1,2,3,\ldots. \end{aligned}$$

Substituting the expansion (3.7) for $\psi^{s,a}(y)$ into (3.9) and using Fourier cosine transformation, we find the integral relations

$$\begin{aligned} B^s(\xi) &= \frac{2}{\pi\xi_1(\sinh\xi_1 b)}\int_d^\infty \zeta^s(u)\cos\xi(u-h)\,du,\\ B^a(\xi) &= \frac{2}{\pi\xi_1(\cosh\xi_1 b)}\int_d^\infty \zeta^a(u)\cos\xi(u-h)\,du. \end{aligned}$$

Fluid pressure is continuous across the line $x = b$ for all $y \in (0,c)\cup(d,\infty)$, that is,

$$\psi^{s,a}(b-0,y) = \psi^{s,a}(b+0,y),\ \ y\in(0,c)\cup(d,\infty).$$

This matching condition ultimately yields the first-kind Fredholm-type integral equations

$$\int_L \zeta_1^{s,a}(u)\mathcal{M}^{s,a}(y,u)\,du = e^{-Ky},\ \ y\in L=(0,c)\cup(d,\infty), \tag{3.11}$$

where

$$\zeta_1^{s,a}(u) = \frac{\zeta^{s,a}(u)}{(1+\mathcal{R}^{s,a})},$$

$$\mathcal{M}^s(y,u) = \begin{cases} -\dfrac{4\alpha_0}{r_0}\dfrac{\cot r_0 b}{\delta_0}V(y,u;\alpha_0) + \displaystyle\sum_{n=1}^{\infty}\frac{4\alpha_n}{\delta_n}\frac{\coth r_n b}{r_n}V(y,u;\alpha_n) & \text{for } 0<u,y<c,\\ \dfrac{2}{\pi}\displaystyle\int_0^\infty \frac{S(\xi,u)S(\xi,y)}{\xi_1(\xi^2+K^2)}\,d\xi + \frac{2}{\pi}\int_0^\infty \frac{\coth\xi_1 b}{\xi_1}W(\xi,y,u)\,d\xi & \text{for } d<u,y<\infty, \end{cases}$$

https://doi.org/10.1017/S144618112510014X Published online by Cambridge University Press

with

$$\begin{aligned} V(y,u;\alpha_0) &= \cosh[\alpha_0(h-y)]\cosh[\alpha_0(h-u)],\\ V(y,u;\alpha_n) &= \cos[\alpha_n(h-y)]\cos[\alpha_n(h-u)],\\ W(\xi,y,u) &= \cos[\xi(y-h)]\cos[\xi(u-h)],\\ \delta_0 &= 2\alpha_0 h + \sinh 2\alpha_0 h,\\ \delta_n &= 2\alpha_n h + \sin 2\alpha_n h. \end{aligned}$$

It should be noted that the expression of $\mathcal{M}^a(y,u)$ is obtained by replacing "cot" by "$-\tan$" and "coth" by "tanh" in $\mathcal{M}^s(y,u)$. Next, the substitution of the solution $\zeta^{s,a}(u) = (1+R^{s,a})\zeta_1^{s,a}(u)$ into (3.10) gives rise to

$$\int_0^c \zeta_1^{s,a}(u)e^{-Ku}\,du + \int_d^\infty \zeta_1^{s,a}(u)e^{-Ku}\,du = \mathcal{P}^{s,a}, \tag{3.12}$$

where

$$\mathcal{P}^{s,a} = -\frac{i\cos\alpha}{2}\frac{1-R^{s,a}}{1+R^{s,a}}.$$

The real valued nature of the kernels $\mathcal{M}^{s,a}(y,u)$ implies that $\zeta_1^{s,a}(u)$ have a similar nature to the integral equation (3.11). As such, the relation (3.12) shows that $\mathcal{P}^{s,a}$ are also real valued. The integral expressions of $\mathcal{P}^{s,a}$ shall be evaluated once the solutions of the integral equation (3.11) are obtained. Subsequently, the required wave reflection and transmission coefficients can be estimated from the expressions

$$|R| = \frac{|1+(2\sec\alpha)^2\mathcal{P}^s\mathcal{P}^a|}{\sqrt{\{1+(2\mathcal{P}^s\sec\alpha)^2\}\{(1+(2\mathcal{P}^a\sec\alpha)^2\}}},$$

$$|T| = \frac{2|\mathcal{P}^s-\mathcal{P}^a|\sec\alpha}{\sqrt{\{1+(2\mathcal{P}^s\sec\alpha)^2\}\{(1+(2\mathcal{P}^a\sec\alpha)^2\}}},$$

satisfying the energy conservation equation $|R|^2+|T|^2=1$.

3.1. Limiting cases From the wave scattering problem of the H-shaped breakwater, two different shapes of the breakwater are deduced by applying certain limits in the breakwater's parameters.

(i) When $c\to h$, the breakwater changes to a submerged $\sqcap$-shaped breakwater for which the integral equations (3.11) shall be solved for solution in the domain $(0,h)\cup(d,\infty)$.

(ii) When $d\to h$, the breakwater changes to a submerged $\sqcup$-shaped breakwater for which the integral equations (3.11) shall be solved for solution in the domain $(0,c)\cup(h,\infty)$.

The water-wave scattering by these breakwaters is also investigated in this paper.

https://doi.org/10.1017/S144618112510014X Published online by Cambridge University Press

4. Approximate solution of the integral equations

In this section, the Galerkin approximation technique is illustrated to solve the integral equations (3.11) associated with wave scattering by the H-shaped breakwater. This approximation is constructed by using simple polynomials multiplied by a suitable weight function. We choose $\zeta_1^{s,a}(y)$ as

$$\zeta_1^{s,a}(y) = \begin{cases} \left\{1 - \dfrac{y}{c}\right\}^{-1/2} \displaystyle\sum_{p=0}^{N} \alpha_p^{s,a} e^{-K(p+1)y} \left(\frac{y}{c}\right)^p & \text{for } 0 < y < c, \\ \left\{\dfrac{y}{d} - 1\right\}^{-1/2} \displaystyle\sum_{p=0}^{N} \beta_p^{s,a} e^{-K(p+1)y} \left(\frac{y}{d}\right)^p & \text{for } d < y < \infty, \end{cases} \tag{4.1}$$

where $\{1 - y/c\}^{-1/2}$ and $\{y/d - 1\}^{-1/2}$ are the weight functions, N is any nonnegative integer, and $\alpha_p^{s,a}$ and $\beta_p^{s,a}$ are unknown constants. Here, $(y/c)^p e^{-K(p+1)y}$ and $(y/d)^p e^{-K(p+1)y}$ are the basis functions. The approximation is chosen based on the behaviour of $\zeta^{s,a}(y)$ at the edges $y = c$ and $y = d$. Note that the exponential term $e^{-K(p+1)y}$ in the expansion preserves the decay properties of Laguerre functions, which can be used alternatively. With this exponential term, rapid convergence of the series shall be achieved with a few terms in the expansion (4.1) which, in turn, shows the accuracy of the method.

We rewrite $\zeta_1^{s,a}(y)$ as

$$\zeta_1^{s,a}(y) = \begin{cases} \displaystyle\sum_{p=0}^{N} \alpha_p^{s,a} \psi_{1p}(y), & 0 < y < c, \\ \displaystyle\sum_{p=0}^{N} \beta_p^{s,a} \psi_{2p}(y), & d < y < \infty, \end{cases} \tag{4.2}$$

where

$$\psi_{1p}(y) = \left\{1 - \left(\frac{y}{c}\right)\right\}^{-1/2} e^{-K(p+1)y} \left(\frac{y}{c}\right)^p, \quad \psi_{2p}(y) = \left\{\left(\frac{y}{d}\right) - 1\right\}^{-1/2} e^{-K(p+1)y} \left(\frac{y}{d}\right)^p. \tag{4.3}$$

We substitute the expansion (4.2) in (3.11) and then multiply by $\psi_{1q}(y)$ and integrate from 0 to c to obtain the linear system of equations

$$\sum_{p=0}^{N} \alpha_p^{s,a} \mathcal{A}_{pq}^{s,a} + \sum_{p=0}^{N} \beta_p^{s,a} \mathcal{B}_{pq}^{s,a} = \mathcal{H}_{1q}, \quad (q = 0, 1, \ldots, N), \tag{4.4}$$

where

$$\mathcal{A}_{pq}^{s} = -\int_0^c \int_0^c \frac{4\alpha_0}{r_0} \frac{\cot r_0 b}{\delta_0} V(y, u; \alpha_0) \psi_{1p}(u) \psi_{1q}(y)\, du\, dy + \sum_{n=1}^{\infty} \int_0^c \int_0^c \frac{4\alpha_n}{\delta_n} \frac{\coth r_n b}{r_n} V(y, u; \alpha_n) \psi_{1p}(u) \psi_{1q}(y)\, du\, dy + \int_0^{\infty} \frac{2\mathcal{I}_1(\xi)}{\pi \xi_1 (\xi^2 + K^2)}\, d\xi,$$

https://doi.org/10.1017/S144618112510014X Published online by Cambridge University Press

$$\mathcal{B}^s_{pq} = \int_0^\infty \frac{\coth(\xi_1 b)\mathcal{J}_1(\xi)}{\xi_1} d\xi + \int_0^\infty \frac{2\mathcal{J}_2(\xi)}{\pi\xi_1(\xi^2+K^2)} d\xi,$$
$$\mathcal{H}_{1q} = \int_0^c e^{-Ky}\psi_{1q}(y)\, dy,$$

with

$$\mathcal{I}_1(\xi) = \int_0^c\int_0^c S(\xi,u)S(\xi,y)\psi_{1p}(u)\psi_{1q}(y)\, du\, dy,$$
$$\mathcal{J}_1(\xi) = \int_0^c\int_d^\infty \cos[\xi(u-h)]\cos[\xi(y-h)]\psi_{2p}(u)\psi_{1q}(y)\, du\, dy,$$
$$\mathcal{J}_2(\xi) = \int_0^c\int_d^\infty S(\xi,u)S(\xi,y)\psi_{2p}(u)\psi_{1q}(y)\, du\, dy.$$

Similarly, we substitute the expansion (4.2) in (3.11) and then multiply by $\psi_{2q}(y)$, and integrate from d to ∞ to obtain the linear system of equations

$$\sum_{p=0}^N \alpha_p^{s,a} C_{pq}^{s,a} + \sum_{p=0}^N \beta_p^{s,a} \mathcal{D}_{pq}^{s,a} = \mathcal{H}_{2q}, \quad (q = 0, 1, \ldots, N), \tag{4.5}$$

where

$$C^s_{pq} = -\int_d^\infty\int_0^c \frac{4\alpha_0}{r_0}\frac{\cot r_0 b}{\delta_0} V(y,u;\alpha_0)\psi_{1p}(u)\psi_{2q}(y)\, du\, dy$$
$$+ \sum_{n=1}^\infty \int_d^\infty\int_0^c \frac{4\alpha_n}{\delta_n}\frac{\coth r_n b}{r_n} V(y,u;\alpha_n)\psi_{1p}(u)\psi_{2q}(y)\, du\, dy + \int_0^\infty \frac{2\mathcal{I}_2(\xi)}{\pi\xi_1(\xi^2+K^2)} d\xi,$$
$$\mathcal{D}^s_{pq} = \int_0^\infty \frac{\coth(\xi_1 b)\mathcal{J}_3(\xi)}{\xi_1} d\xi + \int_0^\infty \frac{2\mathcal{J}_4(\xi)}{\pi\xi_1(\xi^2+K^2)} d\xi,$$
$$\mathcal{H}_{2q} = \int_d^\infty e^{-Ky}\psi_{2q}(y)\, dy,$$

with

$$\mathcal{I}_2(\xi) = \int_d^\infty\int_0^c S(\xi,u)S(\xi,y)\psi_{1p}(u)\psi_{2q}(y)\, du\, dy,$$
$$\mathcal{J}_3(\xi) = \int_d^\infty\int_d^\infty \cos[\xi(u-h)]\cos[\xi(y-h)]\psi_{2p}(u)\psi_{2q}(y)\, du\, dy,$$
$$\mathcal{J}_4(\xi) = \int_d^\infty\int_d^\infty S(\xi,u)S(\xi,y)\psi_{2p}(u)\psi_{2q}(y)\, du\, dy.$$

The expression for $\mathcal{A}^a_{pq}$ and C^a_{pq} shall be obtained by simply replacing "coth" by "tanh" and "cot" by "$-$ tan" in $\mathcal{A}^s_{pq}$ and C^s_{pq}, respectively. The expression for $\mathcal{B}^a_{pq}$ and $\mathcal{D}^a_{pq}$ shall be obtained by simply replacing "coth" by "tanh" in $\mathcal{B}^s_{pq}$ and $\mathcal{D}^s_{pq}$, respectively.

https://doi.org/10.1017/S144618112510014X Published online by Cambridge University Press

Next, the substitution of the expansion equation (4.2) in (3.12) yields

$$\mathcal{P}^{s,a} \approx \mathcal{P}_N^{s,a} = \sum_{p=0}^{N} \alpha_p^{s,a} \mathcal{H}_{1p} + \sum_{p=0}^{N} \beta_p^{s,a} \mathcal{H}_{2p}. \tag{4.6}$$

Thus, after solving the system of equations (4.4) and (4.5) for the unknown constants $\alpha_p^{s,a}$ and $\beta_p^{s,a}$ ($p = 0, 1, \ldots, N$), these solutions can be used to obtain $\mathcal{P}^{s,a}$ from (4.6). In addition, numerical estimates of the reflection and transmission coefficients $|R|$ and $|T|$ can be found subsequently.

5. Computational results

The solution method with two-term Galerkin approximation (that is, $N = 1$) is considered as it appears to be sufficient here. The computation is carried out with MATHEMATICA programming. The wave reflection and transmission coefficients ($|R|$ and $|T|$) are computed and illustrated graphically with various values of the nondimensional parameters: Kd, b/d, c/d for H-shaped breakwater, where d is the total length of the breakwater; Kd, b/d, h/d for submerged $\sqcap$-shaped breakwater, where d is the total length of breakwater; Kh, b/h, c/h for submerged $\sqcup$-shaped breakwater having the total length h. The effect of these relative parameters on wave scattering is studied. We show the convergence of scattering coefficients with $N = 1$ for different wavenumbers Kd in Table 1. It may be noted that the values of the wavenumber Kd are kept moderate here. For a very high value of the wavenumber (high frequency), the waves will be confined within a thin layer below the free surface (and well above the submerged breakwater) so that most of the incident wave energy will be transmitted and very little will be reflected back. The gravitational constant $g = 9.81\text{m/sec}^2$ is fixed in the calculation. The integrals that arise in the approximate solution of integral equations are evaluated by applying the Gauss–Laguerre quadrature with 11 points. In addition, the horizontal wave force (F_x), vertical wave force (F_y) on the breakwater and the overturning moment (OTM) of the breakwater are calculated in magnitude by using the nondimensional formulae [22]

$$F_x = \frac{|C_x|}{\rho g A b}, \quad F_y = \frac{|C_y|}{\rho g A b}, \quad OTM = \frac{|M|}{\rho g A b^2}, \tag{5.1}$$

where A is the incident wave amplitude and

$$C_x = -i\rho\omega \int_c^d \{\phi(b+0, y) - \phi(b-0, y)\}\, dy, \tag{5.2}$$

$$C_y = -i\rho\omega \int_0^b \{\phi(x, a+0) - \phi(x, a-0)\}\, dx, \tag{5.3}$$

$$M = -i\rho\omega \int_c^d (y-h)\{\phi(b+0, y) - \phi(b-0, y)\}\, dy. \tag{5.4}$$

https://doi.org/10.1017/S144618112510014X Published online by Cambridge University Press

TABLE 1. Convergence in $|R|$ and $|T|$ of H-shaped breakwater when $h/d = 0.5$, $c/d = 0.01$, $b/d = 1.0$ and $\alpha = 30°$. Three decimal places of accuracy is achieved with $N = 1$.

	$N = 0$			$N = 1$		
Kd	$\|R\|$	$\|T\|$	$\|R\|^2 + \|T\|^2$	$\|R\|$	$\|T\|$	$\|R\|^2 + \|T\|^2$
0.1	0.99980	0.01981	0.99999	0.99976	0.01993	0.99992
0.5	0.97383	0.22728	1.00000	0.97379	0.2274	0.99998
1.0	0.82699	0.56222	1.00000	0.82697	0.56225	1.00000
1.5	0.34343	0.93918	1.00000	0.34338	0.93920	1.00000
2.0	0.46531	0.88515	1.00000	0.46529	0.88516	1.00000

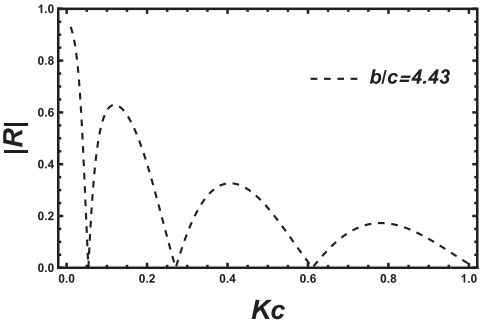


FIGURE 2. Reflection coefficient of Mei and Black [19] for a fully submerged breakwater of rectangular cross section versus wavenumber Kc when $h/c = 1.0$, $\alpha = 0°$, $d = 150$ m.

Note that the symmetric potential function has no effect on the horizontal wave force and the OTM, whereas the vertical wave force depends only on the symmetric potential function.

First, we validate the developed method of solution by producing a known benchmark reflection coefficient ($|R|$) of a fully submerged breakwater of a rectangular cross section whose length is infinite, established by Mei and Black [19]. This case is considered with the H-shaped breakwater taking into account $h/c = 1.0$ and a large value of $d(= 150$ m). This limiting case is reasonable with the H-shaped configuration. The reflection coefficient $|R|$, depicted in Figure 2, almost matches that of [19, Figure 2] concerning a bottom-standing breakwater of infinite length. Thus, the accuracy of the proposed Galerkin approximation is assured with a single term and the correctness of the computation is justified.

Next, we validate our solution method again in a different limiting case that illustrates wave scattering by a thin vertical barrier of finite length fully submerged below the free surface of deep water. This case is concerned with Evans [6], who demonstrated water-wave scattering by a thin submerged vertical plate for normal incident waves ($\alpha = 0°$). We used his wave reflection and transmission coefficients

https://doi.org/10.1017/S144618112510014X Published online by Cambridge University Press

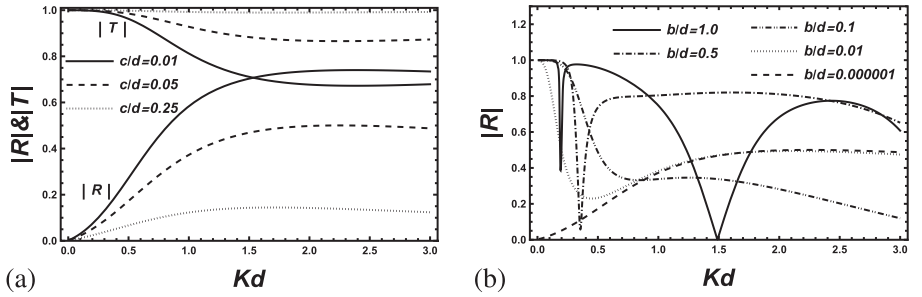


FIGURE 3. (a) Reflection and transmission coefficients as in [6] when $b/d = 10^{-6}$. (b) Reflection coefficients when $c/d = 0.05$ versus wavenumber Kd with $h/d = 0.5$ and $\alpha = 0°$.

($|R|$, $|T|$) to validate our method, illustrated in Figure 3(a). The H-type breakwater shrinks to a thin barrier when $b/d = 10^{-6}$, which is sufficient to show Evans' [6] scattering coefficients for $c/d = 0.01, 0.05, 0.25$, where $d = 10$ m. In Figure 3(a), the present method is proved to show the reflection and transmission coefficients of Evans exactly. Thus, the correctness of the computation is confirmed from Figure 3(a) in the case of a thin submerged barrier as well.

In addition, Figure 3(b) shows how a variation in the reflection coefficient $|R|$ occurs when the H-shaped breakwater gradually shrinks to a thin vertical barrier ($b/d = 10^{-6}$). This demonstrates that $|R|$ starts from one for the H-shaped breakwater having a certain width, and zero or minimum in $|R|$ occurs for some incident wavelengths. It is to be noticed here that so long as the gap (b/d) remains moderate but small, the H-shaped barrier consists of a pair of thin vertical barriers for which the reflection coefficient $|R|$ is very near to unity for very long waves ($Kd \to 0$) as is well known for two submerged thin vertical barriers [3]. The incident wavelengths of zero reflection gradually vanish as the H-shaped breakwater becomes a thin vertical barrier, and $|R|$ ultimately tends to Evans' reflection curve for $b/d = 10^{-6}$, which starts from zero value. Somewhat analogous behaviour of $|R|$ in the very low wavenumber ($Kd \to 0$) range was observed by Tuck [35] as the depth of the water changes from finite to infinite. Thus, from these observations, we point out that the H-shaped breakwater results in higher wave reflection for the most incident wavelengths.

In the following, we show the computational results of the H-, ⊓- and ⊔-shaped breakwaters. The parameter $d = 10$ m is fixed for all the results presented here.

Considering the gap between the H-shaped breakwater and the free surface is very small, the reflection and transmission coefficients ($|R|$ and $|T|$) are shown in Figure 4 as functions of wavenumber Kd to study the effect of width b/d. Here, we compared our results with that of De et al. [4], who reconsidered the problem of wave scattering by a breakwater consisting of two thin vertical barriers piercing the free surface of deep water without a horizontal plate between them. For numerical results, we set $h/c = 0.5$, $\alpha = 0°$ and $b/d = 1, 3, 5$ as in [4]. According to De et al. [4], increased space between vertical barriers leads to increased oscillation behaviour in the wave

https://doi.org/10.1017/S144618112510014X Published online by Cambridge University Press

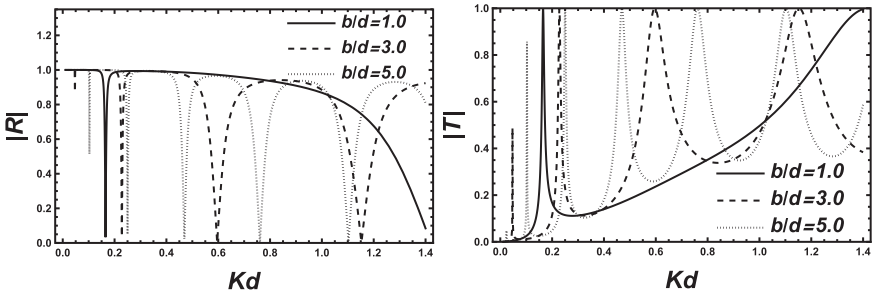


FIGURE 4. Reflection and transmission coefficients of the surface piercing H-shaped breakwater versus wavenumber Kd for $c/d = 10^{-4}$, $h/d = 0.5$ and $\alpha = 0°$.

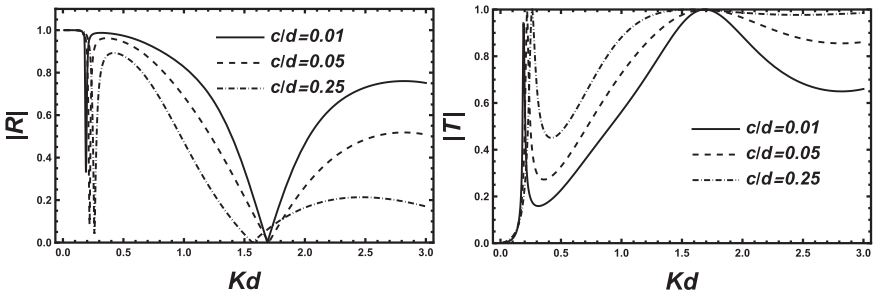


FIGURE 5. Reflection and transmission coefficients of the submerged H-shaped breakwater versus wavenumber Kd for $b/d = 1.0$, $h/d = 0.5$ and $\alpha = 30°$.

reflection coefficient. The breakwater was shown to reflect short waves considerably, but not long waves in deep water. However, the surface-piercing H-shaped breakwater considerably reflects both long and short waves. The horizontal plate between the two vertical plates accounts for this higher reflection. Since more oscillations arise in $|T|$ as the width b/d widens, and cause zero wave reflection or full wave transmission at some wavelengths, the H-shaped breakwater with smaller values of b/d may be employed to achieve low wave transmission.

In Figure 5, we plot the reflection and transmission coefficients ($|R|$ and $|T|$) versus wavenumber Kd for the effect of the gap (c/d) between the H-shaped breakwater and the free surface when $b/d = 1.0$ and $h/d = 0.5$. As expected, wider gaps allow more waves to be transmitted, and, as a result, they yield less wave reflection. Furthermore, it reveals that a few incoming long waves fully transmit over the H-type breakwater. In spite of this, incoming waves of almost all wavelengths are greatly attenuated by this breakwater.

Figure 6 depicts the reflection and transmission coefficients ($|R|$ and $|T|$) versus the wavenumber Kd for different incident wave angles α when $b/d = 1.0$, $c/d = 0.25$ and $h/d = 0.5$. It illustrates that incident waves of higher angles are reflected greatly, except at a few wavelengths.

https://doi.org/10.1017/S144618112510014X Published online by Cambridge University Press

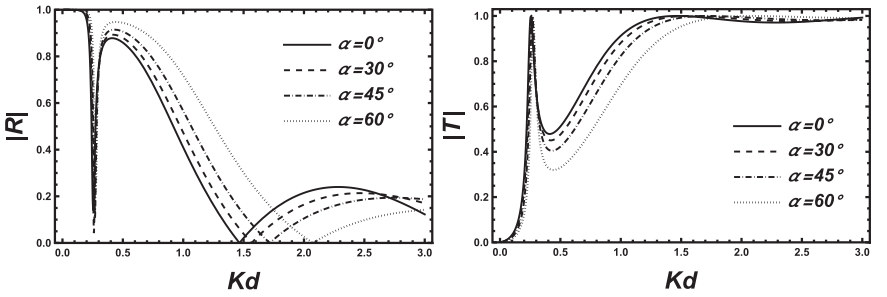


FIGURE 6. Reflection and transmission coefficients of the submerged H-shaped breakwater versus wavenumber Kd for $b/d = 1.0$, $c/d = 0.25$ and $h/d = 0.5$.

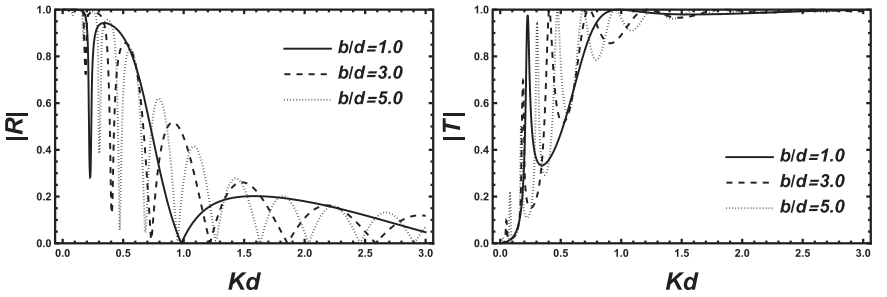


FIGURE 7. Reflection and transmission coefficients of submerged ⊓-shaped breakwater versus wavenumber Kd for $h/d = 0.25$, $\alpha = 30°$.

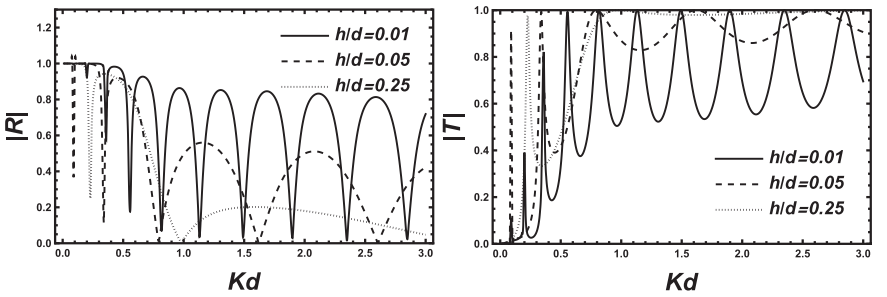


FIGURE 8. Reflection and transmission coefficients of submerged ⊓-shaped breakwater versus wavenumber Kd for $b/d = 1.0$, $\alpha = 30°$.

Figures 7 and 8 demonstrate the reflection and transmission coefficients of submerged ⊓-shaped breakwater versus wavenumber Kd when the width b/d varies, and the gap h/d between the free surface and the breakwater varies, respectively. Like the H-shaped breakwater, the ⊓-shaped breakwater shows higher wave reflection and lower wave transmission in an oscillatory manner with varying width b/d. However, the ⊓-shaped one shows the scattering coefficients in an oscillatory manner when h/d also changes. This is not the case with the H-shaped breakwater. Furthermore,

https://doi.org/10.1017/S144618112510014X Published online by Cambridge University Press

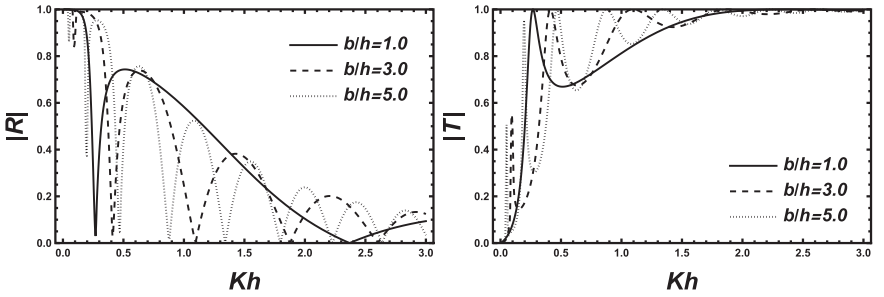


FIGURE 9. Reflection and transmission coefficients of submerged ⊔-shaped breakwater versus wavenumber Kh for $c/h = 0.25$, $\alpha = 30°$.

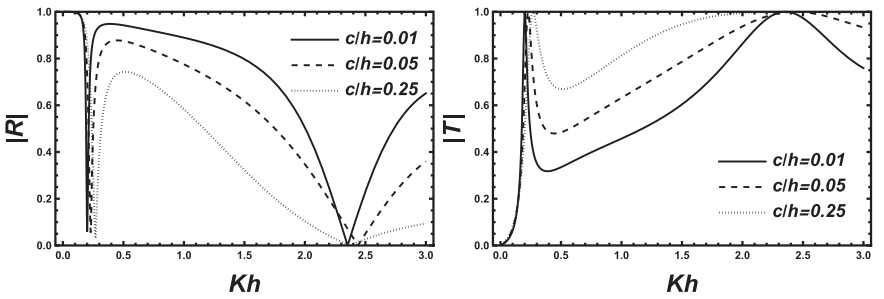


FIGURE 10. Reflection and transmission coefficients of submerged ⊔-shaped breakwater versus wavenumber Kh for $b/h = 1.0$, $\alpha = 30°$.

a comparison of Figure 7 with Figure 8 reveals that the change in h/d is apparently more effective than the change in width b/d of this type of breakwater for wave attenuation.

The reflection and transmission coefficients of ⊔-shaped breakwater are depicted with wavenumber Kh for the varying width b/h in Figure 9 and for the varying gap c/h in Figure 10. The scattering performance of ⊔-shaped breakwater is similar to that of H-shaped breakwater. However, a comparison of Figure 10 with Figure 5 reveals that the ⊔-shaped breakwater reflects short waves considerably more than the H-shaped breakwater. This results in even more reduction in wave transmission.

Figure 11 shows the wave forces and the overturning moment when the width of the H-shaped piercing surface breakwater (b/d) changes. These physical quantities correspond to the wave scattering coefficients described in Figure 4. It reveals that the wider H-breakwater undergoes a lesser horizontal force (F_x) and vertical force (F_y) due to the oscillatory behaviour of the scattering coefficients shown in Figure 4. The incident wavelengths of a minimum wave reflection account for zero horizontal force. Furthermore, only smaller frequency waves cause a higher vertical force. The consequent OTM of the H-breakwater reduces with the increase in its width. Hence, a wider H-breakwater has lesser OTM, which is evident from the fact that a larger-size

https://doi.org/10.1017/S144618112510014X Published online by Cambridge University Press

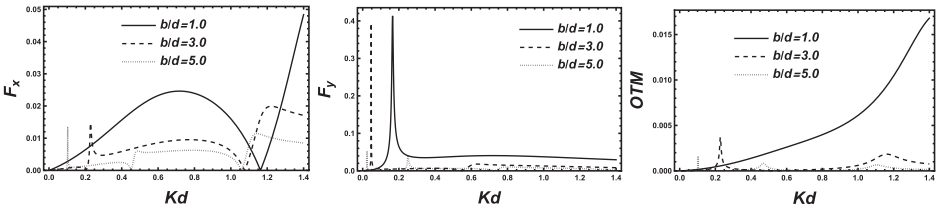


FIGURE 11. Horizontal force (F_x), vertical force (F_y) and OTM of the surface piercing H-shaped breakwater associated with Figure 4.

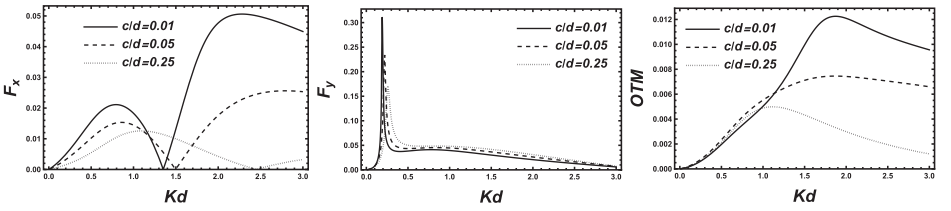


FIGURE 12. Horizontal force (F_x), vertical force (F_y) and overturning moment (OTM) of the submerged H-shaped breakwater associated with Figure 5.

object needs much effort to spin. Generally, high-frequency waves cause a higher OTM, and low-frequency waves cause a lower OTM. Figure 11 is consistent with this fact. Ultimately, it turns out that the overall OTM of the free-surface H-breakwater with larger widths is much less.

Figure 12 shows the wave forces and OTM when the submerged gap of H-shaped breakwater (c/d) changes. These physical quantities correspond to the wave scattering coefficients described in Figure 5. An increase in the submergence gap (c/d) leads to a reduction in the horizontal force (F_x) and an increment in the vertical force (F_y), which is due to the reduction in wave reflection or increased transmission in waves as is evident from Figure 5. Furthermore, the breakwater does not undergo horizontal force where the wave reflection coefficient is zero or minimum. In other words, the breakwater undergoes a higher vertical force where the wave transmission coefficient tends to a maximum. This situation is consistent with wave scattering and wave forces. The resulting OTM reduces with the submergence gap (c/d) since the horizontal force (F_x) reduces. Higher horizontal wave force leads to higher OTM.

Figures 13 and 14 present the effect of the submerged gap lengths of ⊓- and ⊔-shaped breakwaters on wave forces and OTM in the wave scattering situation illustrated in Figures 8 and 10, respectively. The variations in the physical quantities of ⊔-breakwater are analogous to those of the H-breakwater as in Figure 12. However, these physical quantities possess an oscillatory nature in the case of ⊓-breakwater because of the highly oscillatory reflection coefficient, depicted in Figure 8. In addition, these quantities are higher at low-frequency incident waves and

https://doi.org/10.1017/S144618112510014X Published online by Cambridge University Press

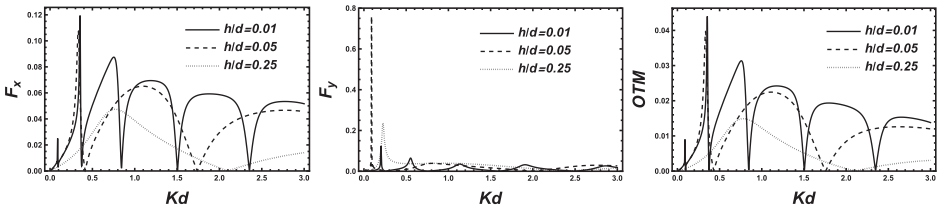


FIGURE 13. Horizontal force (F_x), vertical force (F_y) and overturning moment (OTM) of the submerged ⊓-shaped breakwater associated with Figure 8.

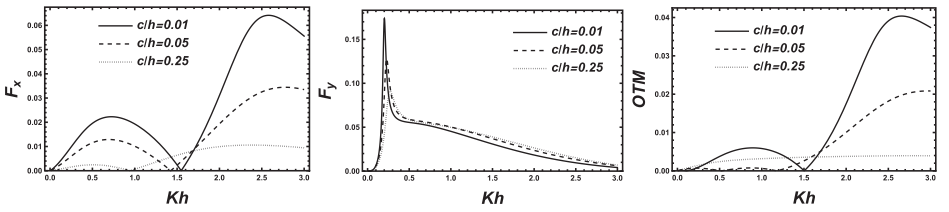


FIGURE 14. Horizontal force (F_x), vertical force (F_y) and overturning moment (OTM) of the submerged ⊔-shaped breakwater associated with Figure 10.

lower at high-frequency incident waves, which account for the reversed breakwater configuration.

Finally, from the above results, one can determine the effect of wave incident angles on wave forces and OTM. Since the increase in wave angle results in higher wave reflection or lower wave transmission, as shown in Figure 6, higher wave angles account for a higher horizontal force and a lower vertical force, and therefore a higher OTM.

6. Conclusions

In this paper, wave scattering by an H-shaped breakwater submerged in water of infinite depth is studied by integral equation formulation. An approximate solution of the first-kind Fredholm-type integral equation is obtained through the Galerkin approximation. The coefficients of wave reflection and transmission are calculated by using the approximate solution of integral equations. These scattering quantities are graphically depicted with breakwater parameters against the wavenumber. First, the developed method replicates the known results in limiting cases associated with water-wave scattering by a thin submerged finite plate and a submerged long rectangular beam. Next, the wave scattering performance of H-, ⊓- and ⊔-shaped breakwaters is investigated. The H-shaped breakwater, whether in a surface-piercing or fully submerged position, considerably reflects both long and short waves. It is in contrast to the traditional breakwater system, which consists of two vertical barriers without a horizontal plate that reflects short waves in the surface piercing position

https://doi.org/10.1017/S144618112510014X Published online by Cambridge University Press

and long waves in the fully submerged position. When the width of the breakwater is greater than the total submergence length of the H-shaped breakwater, the waves are strongly reflected for most incident wavelengths. The shorter submerged lengths of the H-type breakwater from the free surface show higher wave reflection. However, zero or minimum reflection still occurs for certain incident wavenumbers in the case of H-shaped breakwater, as in the case of dual vertical barriers without a horizontal plate. Such wavenumbers may disappear for asymmetric H-shaped breakwater as in the case of vertical barriers of unequal length.

In limiting cases, wave scattering by submerged ⊔- and ⊓-shaped breakwaters is also studied. The ⊔-shaped breakwater has reflective characteristics similar to the H-shaped breakwater. However, the submerged ⊓-shaped one shows oscillations in the wave reflection coefficient when its width and submergence gap change. In addition, the wave forces and the resulting OTM are also calculated. A reduction in horizontal and vertical forces and OTM is observed with an increase in the width of the breakwater. However, the horizontal force is reduced and the vertical force is enhanced when the submergence gap of the breakwater increases. OTM is proportional to the horizontal force in all cases, as expected. Depending on site locations and wave scattering requirements, these structures may be opted for as breakwaters.

Acknowledgments

R. B. Kaligatla acknowledges the funding support of the Science and Engineering Research Board, Government of India, under the MATRICS project with grant No. MTR/2022/000113. The authors thank anonymous reviewers for their comments and suggestions for improving the presentation of the manuscript.

References

[1] A. Chakrabarti, S. Banerjea, B. N. Mandal and T. Sahoo, "A unified approach to problems of scattering of surface water waves by vertical barriers", *J. Aust. Math. Soc. Ser. B* **39** (1997) 93–103; doi:10.1017/S0334270000009231.

[2] E. D. Christensen, H. B. Bingham, A. P. S. Friis, A. K. Larsen and K. L. Jensen, "An experimental and numerical study of floating breakwaters", *Coastal Eng.* **137** (2018) 43–58; doi:10.1016/j.coastaleng.2018.03.002.

[3] S. De, B. N. Mandal and A. Chakrabarti, "Water-wave scattering by two submerged plane vertical barriers—Abel integral-equation approach", *J. Engrg. Math.* **65** (2009) 75–87; doi:10.1007/s10665-009-9265-3.

[4] S. De, B. N. Mandal and A. Chakrabarti, "Use of Abel integral equations in water wave scattering by two surface-piercing barriers", *Wave Motion* **47** (2010) 279–288; doi:10.1016/j.wavemoti.2009.12.002.

[5] Z. Deng, L. Wang, X. Zhao and Z. Huang, "Hydrodynamic performance of a T-shaped floating breakwater", *Appl. Ocean Res.* **82** (2019) 325–336; doi:10.1016/j.apor.2018.11.002.

[6] D. V. Evans, "Diffraction of water waves by a submerged vertical plate", *J. Fluid Mech.* **40** (1970) 433–451; doi:10.1017/S0022112070000253.

[7] D. V. Evans and C. A. N. Morris, "Complementary approximations to the solution of a problem in water waves", *IMA J. Appl. Math.* **10** (1972) 1–9; doi:10.1093/imamat/10.1.1.

https://doi.org/10.1017/S144618112510014X Published online by Cambridge University Press

[8] M. R. Gesraha, "Analysis of Π shaped floating breakwater in oblique waves: I. Impervious rigid wave boards", *Appl. Ocean Res.* **28** (2006) 327–338; doi:10.1016/j.apor.2007.01.002.
[9] K. Günaydın and M. S. Kabdaşlı, "Performance of solid and perforated U-type breakwaters under regular and irregular waves", *Ocean Eng.* **31** (11–12) (2004) 1377–1405; doi:10.1016/j.oceaneng.2004.02.002.
[10] T. H. Havelock, "Forced surface-waves on water", *London, Edinburgh, Dublin Philos. Mag. J. Sci.* **8**(51) (1929) 569–576; doi:10.1080/14786441008564913.
[11] R. J. Jarvis, "The scattering of surface waves by two vertical plane barriers", *J. Inst. Math. Appl.* **7** (1971) 207–215.
[12] R. B. Kaligatla, S. Singh and B. N. Mandal, "Wave scattering by Pi-type breakwater floating in deep water", *J. Engrg. Math.* **143** (2023) article ID: 7; doi:10.1007/s10665-023-10301-7.
[13] J. T. Kirby and R. A. Dalrymple, "Propagation of obliquely incident water waves over a trench", *J. Fluid Mech.* **133** (1983) 47–63; doi:10.1017/S0022112083001780.
[14] H. Levine and E. Rodemich, "Scattering of surface waves on an ideal fluid", *Appl. Math. Stat. Lab., Stanford Univ.* **49** (1958) 65–74.
[15] C. M. Linton and P. McIver, *Handbook of mathematical techniques for wave/structure interactions* (CRC Press, Boca Raton, FL, 2001); doi:10.1201/9781420036060.
[16] B. N. Mandal and A. Chakrabarti, *Water wave scattering by barriers*, 4th edn (WIT Press, Southampton, UK, 2000); https://api.semanticscholar.org/CorpusID:92876695.
[17] E. Masoudi and L. Gan, "Diffraction waves on general two-legged rectangular floating breakwaters", *Ocean Eng.* **235** (2021) article ID: 109420; doi:10.1016/j.oceaneng.2021.109420.
[18] P. McIver, "Scattering of water waves by two surface-piercing vertical barriers", *IMA J. Appl. Math.* **35**(3) (1985) 339–355; doi:10.1093/imamat/35.3.339.
[19] C. C. Mei and J. L. Black, "Scattering of surface waves by rectangular obstacles in waters of finite depth", *J. Fluid Mech.* **38** (1969) 499–511; doi:10.1017/S0022112069000309.
[20] C. H. Midya, M. Kanoria and B. N. Mandal, "Scattering of water waves by inclined thin plate submerged in finite-depth water", *Arch. Appl. Mech.* **71** (2001) 827–840; doi:10.1007/s004190100187.
[21] S. C. Mohapatra, I. B. da Silva Bispo, Y. Guo and C. Guedes Soares, "Analysis of wave-induced forces on a floating rectangular box with analytical and numerical approaches", *J. Marine Sci. Appl.* **23**(1) (2024) 113–126; doi:10.1007/s11804024003857.
[22] R. A. Naftzger and S. K. Chakrabarti, "Scattering of waves by two-dimensional circular obstacles in finite water depths", *J. Ship Res.* **23** (1979) 32–42; doi:10.5957/jsr.1979.23.1.32.
[23] N. J. Nederstigt, "The deep water breakwater", Offshore Engineering Thesis, TU Delft, 1996; https://resolver.tudelft.nl/uuid:0382c8c1-c10a-474a-9576-02632d3eaa02.
[24] S. Neelamani and R. Rajendran, "Wave interaction with T-type breakwaters", *Ocean Eng.* **29** (2002) 151–175; doi: 10.1016/S0029-8018(00)00060-3.
[25] S. Neelamani and M. Vedagiri, "Wave interaction with partially immersed twin vertical barriers", *Ocean Eng.* **29** (2002) 215–238; doi:10.1016/S0029-8018(00)00061-5.
[26] C. S. Nishad, K. G. Vijay, S. Neelamani and J. T. Chen, "Dual BEM for wave scattering by an H-type porous barrier with nonlinear pressure drop", *Eng. Anal. Bound. Elem.* **131** (2021) 280–294; doi:10.1016/j.enganabound.2021.06.011.
[27] A. Panda, D. Karmakar and M. Rao, "Hydrodynamic analysis of an H-shaped pile-restrained floating breakwater combined with a pair of vertical barriers", *Ocean Eng.* **298** (2024) article ID: 117152; doi:10.1016/j.oceaneng.2024.117152.
[28] N. F. Parsons and P. A. Martin, "Scattering of water waves by submerged plates using hypersingular integral equations", *Appl. Ocean Res.* **14** (1992) 313–321; doi:10.1016/0141-1187(92)90035-I.
[29] D. Porter, "The transmission of surface waves through a gap in a vertical barrier", *Proc. Cambridge Philos. Soc.* **71** (1972) 411–421; doi:10.1017/S0305004100050647.
[30] R. Porter and D. V. Evans, "Complementary approximations to wave scattering by vertical barriers", *J. Fluid Mech.* **294** (1995) 155–180; doi:10.1017/S0022112095002849.
[31] R. Roy, U. Basu and B. N. Mandal, "Oblique water wave scattering by two unequal vertical barriers", *J. Engrg. Math.* **97** (2016) 119–133; doi:10.1007/s10665-015-9800-3.

https://doi.org/10.1017/S144618112510014X Published online by Cambridge University Press

[32] P. Ruol, L. Martinelli and P. Pezzutto, "Formula to predict transmission for π-type floating breakwaters", *J. Waterway Port Coastal Ocean Eng.* **139** (2013) 1–8; doi:10.1061/(ASCE)WW.1943-5460.0000153.

[33] S. Singh, R. B. Kaligatla and B. N. Mandal, "Wave scattering by Pi-shaped breakwaters in finite depth water", *Appl. Ocean Res.* **148** (2024) article ID: 104014; doi:10.1016/j.apor.2024.104014.

[34] H. M. Teh,"Hydraulic performance of free surface breakwaters: a review", *Sains Malays.* **42** (2013) 1301–1310; https://khub.utp.edu.my/scholars/id/eprint/3490.

[35] E. O. Tuck, "Matching problems involving flow through small holes", *Adv. Appl. Mech.* **15** (1975) 89–158; doi:10.1016/S0065-2156(08)70056-5.

[36] F. Ursell, "The effect of a fixed vertical barrier on surface waves in deep water", *Proc. Cambridge Philos. Soc.* **43** (1947) 374–382; doi:10.1017/S0305004100023604.

[37] C. M. Wang and H. P. Nguyen, "Floating breakwaters: sustainable solution for creating sheltered sea space", in: *Proceedings of the second international conference on sustainable civil engineering and architecture ICSCEA 2021, Singapore* (Springer Nature, Singapore, 2022); doi:10.1007/978-981-19-3303-5-1.

https://doi.org/10.1017/S144618112510014X Published online by Cambridge University Press